Electronic structure of $HfN_{0.93}(100)$ studied by angle-resolved photoemission

J. Lindström, L. I. Johansson, P. E. S. Persson, and A. Callenås
Department of Physics and Measurement Technology, Linköping University, S-581 83 Linköping, Sweden

D. S. L. Law
Daresbury Laboratory, Science and Engineering Research Council, Daresbury, Warrington WA4 4AD, United Kingdom

A. N. Christensen
Department of Chemistry, Aarhus University, DK-8000 Aarhus C, Denmark
(Received 8 July 1988)

An experimental and theoretical study of the electronic structure of HfN is reported. Results from angle-resolved photoemission experiments on $HfN_{0.93}(100)$ are presented and interpreted with use of calculated results. The bulk-band structure of stoichiometric HfN was calculated relativistically and nonrelativistically using the linear augmented-plane-wave method. Predicted band locations and dispersions along the $\Gamma-X$ direction are compared with experimental results. In general the experiment indicates smaller bandwidths and locates the bands deeper below the Fermi level than the calculated values. Calculations of photoemission spectra, made nonrelativistically, are also reported and these spectra are found to reflect the recorded spectra fairly well.

INTRODUCTION

Several theoretical[1] and experimental[2] studies of the electronic structure of the group-IV*B* and -V*B* transition-metal carbides and nitrides (TMCN's) have been published. These compounds have attracted much attention due to the unusual combination of properties they exhibit.[3] Their properties are characteristic of both covalently bonded and metallic materials, i.e., extreme hardness and high melting point together with good thermal and electrical conductivity. These properties are closely related to the electronic-structure and therefore band-structure studies of these materials using photoelectron spectroscopy seem well motivated.

The electronic structure of hafnium nitride, HfN, has earlier only been investigated using angle-integrated photoelectron spectroscopy in the x-ray regime,[4-6] which mainly provides information about the total density of occupied states. In this paper results from angle-resolved photoemission experiments on a $HfN_{0.93}(100)$ surface are presented. Photon energies in the range 17–56 eV were utilized and spectra were recorded at normal electron emission, thus allowing an experimental mapping of the band structure along the $\Gamma-X$ direction. The band structure of stoichiometric HfN was calculated, both relativistically and nonrelativistically, along $\Gamma-X$. This enabled a comparison between theoretical and experimental band dispersions and energy locations to be made. Angle-resolved photoemission spectra were also calculated nonrelativistically using the potential generated in the band-structure calculation. The experimental and theoretical results are below compared and discussed.

EXPERIMENTAL DETAILS

The angle-resolved photoemission experiments were performed on beam line 6.2 at the Daresbury Laboratory storage ring. A toroidal-grating monochromator, providing photons in the energy range 17–56 eV, and a VG ADES 400 electron spectrometer, operating at a base pressure of less than 2×10^{-10} Torr, were utilized for the experiments. The monochromator and the analyzer energy resolution were both selected to be better than 0.2 eV, giving a total resolution of about 0.3 eV. The acceptance angle of the electron analyzer was $\pm2°$.

The single crystal of HfN was grown by the zone-annealing technique.[7] A hafnium rod of 99.9% purity was made by zone melting in helium and the rod was then annealed in a nitrogen atmosphere at high pressure. That gave a single crystal with the NaCl structure of bulk composition $HfN_{0.93}$, as determined gravimetrically. The crystal was cut by spark erosion along the (100) plane and polished. It was then mounted on the manipulator with the surface normal in the plane of the analyzer, within $\pm1°$. The crystal was cleaned *in situ* by repeated flash heatings to about 1300 °C. This was found to produce an ordered surface that stayed clean for several hours, as checked by low-energy electron diffraction (LEED) and photoemission. Using LEED the $\langle011\rangle$ azimuth was determined to be parallel to the plane of the analyzer. The polarized synchrotron radiation used had the main part of the electric field vector in the plane of the analyzer. The incidence angle θ_i of the light is below given relative to the surface normal. Spectra were recorded at normal electron emission confining the investigation to the electron energy bands in the $\Gamma-X$ direction of the Brillouin zone.

BAND-STRUCTURE CALCULATION

Self-consistent band-structure calculations along the $\Gamma-X$ symmetry line were done using both the relativistic and nonrelativistic linear augmented-plane-wave method (LAPW).[8] These calculated results were used to interpret the angle-resolved photoemission data and the potential generated was utilized to calculate photoemission spectra

for HfN(100), nonrelativistically.

The self-consistent potential was calculated using 113 unsymmetrized plane waves. The nonspherical contributions to the potential were approximately taken account of by extending the plane waves into the muffin-tin spheres. The wave functions of the core and valence electrons were recalculated in each iteration cycle. The self-consistent criterion applied was that the maximum deviations of eigenvalues between two successive iterations should be better than 1 mRy. The calculation was done within the local-density-functional scheme[9] and the Hedin-Lundqvist approximation[10] for the exchange and correlation potential has been used. This self-consistent potential was then used to calculate the band structure.

In the LAPW method[11] the radial wave functions inside the atomic spheres are expanded around an energy parameter E_l. The energy eigenvalues are most accurate within an energy range of 1 Ry around the E_l values. The E_l values used in the calculations are presented in Table I. The resulting band structure was obtained by combining energy eigenvalues for the different energy regions. The result is shown in Fig. 1. In the relativistic band-structure calculation 2×89 basis functions have been used, while 89 basis functions were used nonrelativistically. The first nine spherical harmonics were included in the expansion of the wave functions inside the atomic spheres. Since the calculations are time consuming the relativistic bands were only calculated for 17 **k** points along $\Gamma-X$, while 65 **k** points were used nonrelativistically. This gave the relativistic bands in Fig. 1 a more irregular appearance since straight lines have been drawn between the eigenvalues. The major difference between the two band-structure calculations, aside from the spin-orbit splitting of the doubly degenerate nonrelativistic states, is the shift to lower eigenvalues in the relativistic case. The relativistic bands are generally found at lower-energies than their nonrelativistic counterparts. In Table II relativistic effects in the band structure are

TABLE I. The energy parameters E_l used in the different energy regions in the relativistic band-structure calculation. The energies are given with respect to the muffin-tin zero in Ry.

Region	l	E_l(N sphere)	l	E_l(Hf sphere)
1	0	−0.144	0	1.120
	1	0.551	1	−1.175
	2	0.569	2	0.804
	3	−0.062	3	−0.475
	4	−0.135	4	0.135
	5	−0.082	5	0.223
	6	−0.050	6	0.192
	7	−0.491	7	−0.160
	8	−0.231	8	0.506
2		all $E_l=0.5$		
3		all $E_l=1.5$		
4		all $E_l=2.5$		
5		all $E_l=3.5$		
6		all $E_l=4.5$		

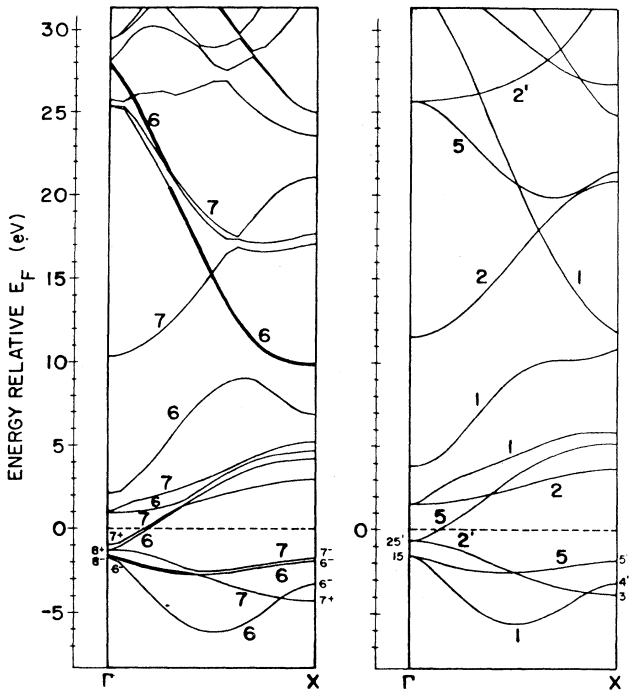

FIG. 1. Band structure of $HfN_{1.0}$ calculated along the $\Gamma-X$ direction using the (a) relativistic and (b) nonrelativistic LAPW (linear augmented-plane-wave) method.

presented for the high-symmetry points Γ and X. It is seen in Table II and Fig. 1 that of the occupied bands close to the Fermi level the Hf $5d$ bands are more affected by relativistic effects than the N $2p$ bands, which is expected. The N $2p$ band with Δ_5 symmetry is split ($\Delta_5\rightarrow\Delta_6,\Delta_7$) but the shift in energy is very small. In addition, more gaps appear in the relativistic band structure, since bands of the same symmetry are not allowed to cross each other. However, at the higher energies in Fig. 1 some of the gaps are probably not real but are features of the plot, since only 17 **k** points had been calculated along $\Gamma-X$.

CALCULATED SPECTRA

Theoretical photoemission spectra were calculated for the stoichiometric composition of the HfN(100) surface. Angle-resolved spectra were calculated within the time-reversed LEED theory[12] using the extended version[13] applicable to binary compounds. The self-consistent potential generated in the LAPW band-structure calculation was used in all layers, and bulk atomic positions were assumed. The surface barrier at the solid-vacuum interface was located to touch the muffin-tin spheres of the metal atoms in the surface layer. The height of the barrier was determined from the experimental work function, $\Phi=3$ eV. The lifetime-broadening parameters, which determine the width of the calculated structures, were chosen to be 0.14 and 2.0 eV for the filled and empty states, respectively. These values have earlier been shown[14,15] to reflect the widths of the structures in the experimental spectra quite well for the TMCN's. The

TABLE II. Relativistic effects on the band structure of HfN. The differences in energy between the high symmetry points specified are given in eV.

N 2*s*	Γ_6^+ (Γ_1)	−0.92	Hf $4f_{7/2}$	Γ_7^- ($\Gamma_{2'}$)	−0.54
	X_6^+ (X_1)	−0.20	Hf $4f_{5/2}$	Γ_7^- ($\Gamma_{2'}$)	−2.42
N 2*p*	Γ_6^- (Γ_{15})	−0.08	Hf 5*d*	Γ_8^+ ($\Gamma_{25'}$)	−0.68
	Γ_8^- (Γ_{15})	0.01		Γ_7^- ($\Gamma_{25'}$)	−0.34
	X_6^- ($X_{4'}$)	−0.11		X_7^+ (X_3)	−0.42
	X_6^- ($X_{5'}$)	−0.11			
	X_7^- ($X_{5'}$)	0.05			

electric field vector of the linearly polarized radiation was chosen to be parallel to the plane of incidence. In the calculated spectra, only relative intensities within each spectrum should be compared, since no corrections for reflection or refraction at the surface have been included in the calculations. Ideal conditions have been assumed, such as a perfect smooth crystal surface and a vanishingly narrow acceptance cone of the analyzer. All the spectra below are calculated for normal electron emission and the energies are given relative the Fermi level.

EXPERIMENTAL RESULTS AND DISCUSSION

Before discussing the experimental band-structure results the importance of including relativistic effects in the treatment of the more localized Hf 4*f* and 5*p* levels is illustrated in Fig. 2, where a wide-scan angle-integrated spectrum recorded at a photon energy of 75 eV is shown. The spin-orbit splitting of the Hf 4*f* and 5*p* levels is clearly observed. The positions obtained for these levels in the relativistic band-structure calculation are indicated by tic marks. The observed splitting of the 4*f* levels, 1.8 eV, is well reproduced by the calculated value of 1.7 eV, but the calculated splitting of the 5*p* levels, 6.1 eV, is smaller than the observed value of 7.4 eV. The position of the 5*p* levels, however, agrees fairly well, while the calculation locates the 4*f* levels approximately 4.5 eV lower in energy then the results observed experimentally.

A previous calculation by Weinberger *et al.*[16] located the 4*f* levels approximately 10 eV closer to the Fermi level. They used the relativistic Korringa-Kohn-Rostoker method (KKR) and the $X\alpha$ exchange approximation. The different methods thus locate the 4*f* levels at opposite sides of the N 2*s* level, which is probably due to the different exchange approximations used (Hedin-Lundqvist and $X\alpha$, respectively). However, the splitting of the 4*f* levels is approximately the same with both methods. The peak expected from the N 2*s* level is not clearly seen in the spectrum. This is probably due to a low cross section at this photon energy and overlapping of the N 2*s* and Hf 4*f* peaks. For the band structure the relativistic effects are considerably smaller than for the more localized Hf 4*f* and 5*p* states, as seen in Figs. 1 and 2. Therefore, in the following we first utilize the calculated nonrelativistic results for interpreting the features observed in the recorded photoemission spectra and thereafter we use the calculated relativistic band structure for a band mapping.

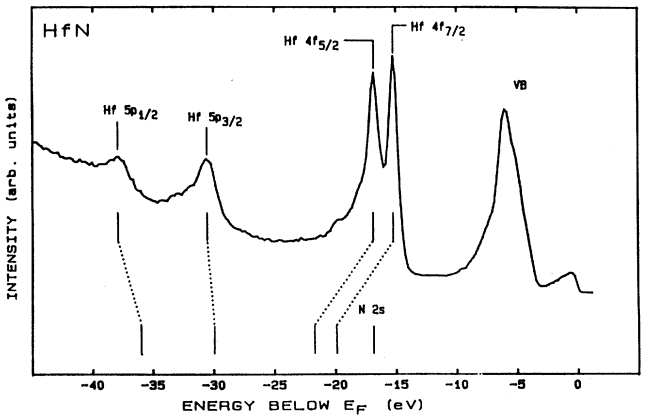

FIG. 2. Angle-integrated spectrum of $HfN_{0.93}(100)$ recorded at a photon energy of 75 eV. The energy levels of Hf 4*f*, Hf 5*p*, and N 2*s*, calculated relativistically, are also indicated in the figure for comparison.

Angle-resolved normal-emission spectra for HfN(100) recorded at two different incidence angles and at three different photon energies are shown in Fig. 3. Four different structures are observed in the spectra and are labeled *A*–*D*. By applying symmetry selection rules[17–20] is it possible to determine the symmetry of the bands from which the peaks originate. At normal emission excitations are only allowed from Δ_1 and Δ_5 initial-state bands to Δ_1 final-state bands; the component of the electric field vector normal to the surface can only excite Δ_1 states and the parallel component only Δ_5 states. Hence, the change in relative intensity between peaks recorded at different incidence angles when using polarized radiation reveals their symmetry character. The changes seen in Fig. 3 show that peaks *A* and *B* originate from states of Δ_5 symmetry and peak *D* from states of Δ_1 symmetry. The polarization dependence of peak *C* is less clear, but tends to indicate that it arises from Δ_1 states. A larger difference between the incidence angles would, of course, have given a clearer polarization dependence, but experimental constraints prevented us from recording normal-emission spectra at an incidence angle smaller than 30°. However, the symmetry assignments agree with results from measurements made using radiation from a resonance lamp where smaller θ_i could be used,[21] giving a clearer polarization dependence for peaks *A* and *D*.

Photoemission spectra recorded at normal electron emission at photon energies between 17 and 38 eV are shown in Figs. 4 and 5. Peak *D* shows clear dispersion at photon energies between 17 and 28 eV, indicating that it originates from transitions from the Δ_1 bulk band. At photon energies exceeding 28 eV peak *D* becomes weaker and broader and its dispersion is thus harder to follow. At photon energies below 24 eV one structure is observed

around -3.5 eV. At larger photon energies this structure splits into two peaks labeled *A* and *B*. Our interpretation is that at smaller photon energies peaks *A* and *B* overlap, but that peak *A* disperses towards the Fermi level with increasing photon energy while peak *B* exhibits no dispersion. We associate peak *A* with transitions from the Δ_5 bulk band. The origin of peaks *B* and *C*, which show no dispersion but a polarization dependence, is discussed below. The corresponding theoretical spectra calculated nonrelativistically are also shown in Figs. 4 and 5. The experimental counterparts to the peaks in the theoretical spectra are in most cases easily identified and the symmetry assignments made above agree with the calculated results. The calculated spectra in Fig. 4 mimic the dispersion of peak *D* fairly well and also explain the behavior of peak *A* in the experimental spectra. Peak *D* is seen to move through a minimum energy position at a photon energy of approximately 22 eV. Upon increasing the photon energy further it then moves back towards smaller binding energy and becomes broader above 26–27 eV in both the experimental and the calculated spectra.

The structure around ~ 3 eV in the calculated spectra, which we associate with peak *A* in the experimental spectra, is seen to disperse slowly towards the Fermi level upon increasing the photon energy from 17 to 27 eV. The intensity at the Fermi level begins to increase at a photon energy of 22 eV, developing into a prominent peak in the calculated 27-eV spectrum. There is also a peak at the Fermi level in the experimental spectra, but the intensity is much lower. The deepest-lying structure in the calculated spectrum at 19 eV photon energy shows a weaker shoulder that becomes relatively more intense as the photon energy increases. At photon energies larger than 26 eV the broad structure actually peaks at the energy location where the shoulder developed. The latter is clearly seen also in Fig. 5, where spectra calculated at photon energies between 28 and 38 eV are presented, showing the lowest-lying structure to remain at constant energy. It seems like this feature in the calculated spectra corresponds to peak *C* in the experimental spectra. They show similar behavior, no dispersion, and a binding energy close to 5 eV.

Features arising from emission from band extrema may appear in the spectra[12,13] and we tentatively ascribe the shoulder appearing in the calculated spectra to such effects. Upon increasing the photon energy a larger portion of the Brillouin zone will be probed experimentally, due to the finite acceptance angle of the analyzer, and the recorded spectra will possibly contain a larger contribution of density-of-states effects. This may explain why at larger photon energies (see Fig. 5) the lowest-lying structure in the experimental spectra is not discernable in the calculated spectra. However, the appearance of peak *B* and the separation of peaks *A* and *B* in the experimental spectra is well reflected in the calculated curves at the largest photon energies, although this might be fortuitous. One-dimensional density-of-states features can also contribute significantly in photoemission spectra if con-

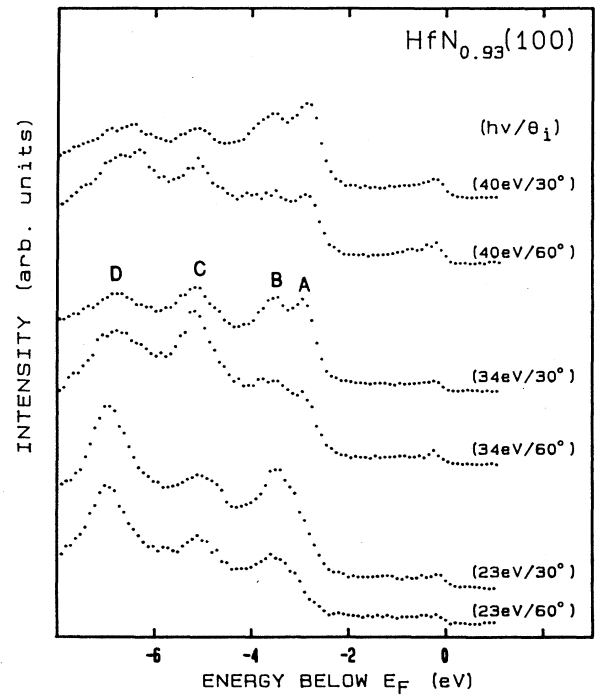

FIG. 3. Normal-emission angle-resolved spectra from $HfN_{0.93}(100)$ recorded at 23, 34, and 40 eV, respectively, and at two different incidence angles θ_i.

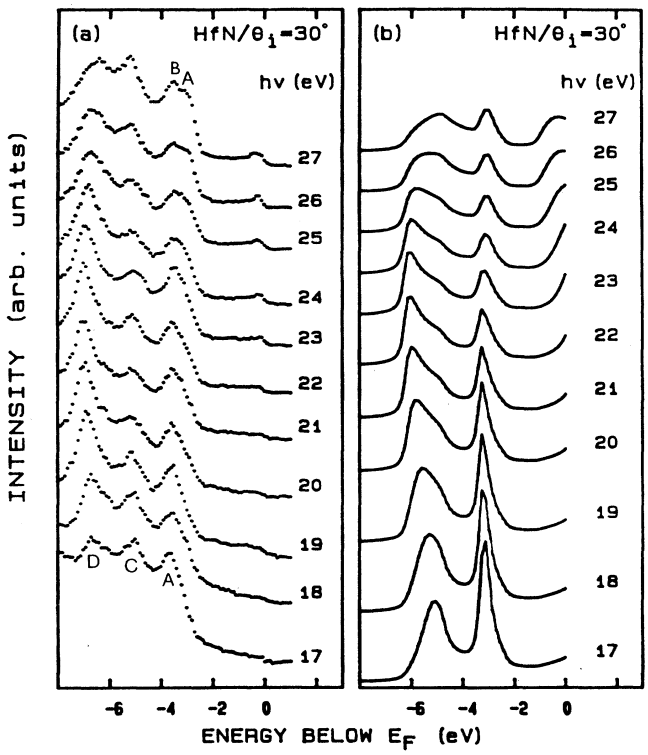

FIG. 4. Angle-resolved normal-emission spectra at $\theta_i = 30°$ and at photon energies in the range 17–27 eV. (a) Experimental spectra from $HfN_{0.93}(100)$. (b) Calculated spectra from $HfN_{1.0}(100)$.

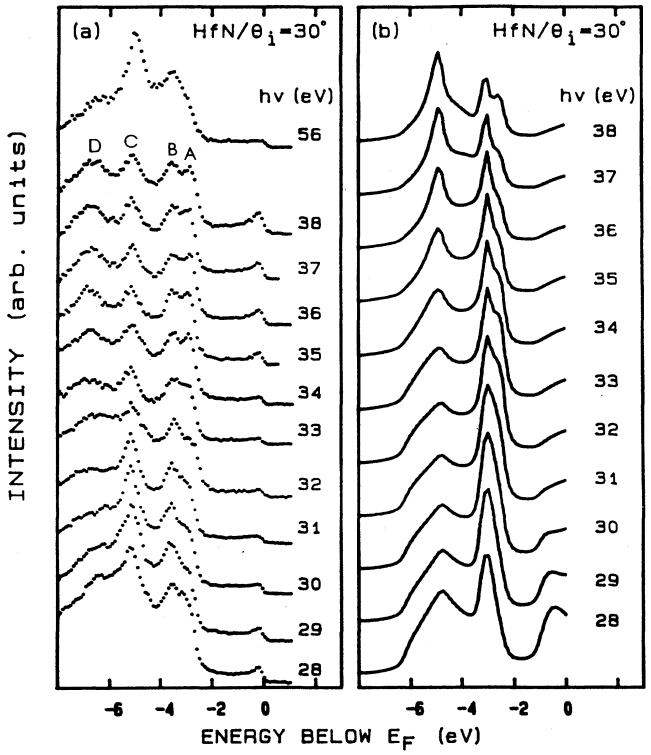

FIG. 5. Angle-resolved normal-emission spectra at $\theta_i = 30°$ and at photon energies in the range 28–38 eV. (a) Experimental spectra from $HfN_{0.93}(100)$. (b) Calculated spectra from $HfN_{1.0}(100)$. Experimental spectrum, recorded at 56 eV, is also shown in (a).

servation of $\mathbf{k}_\perp$ is relaxed due to a short photoelectron escape depth.[22] This may actually be the case in HfN since the heavy Hf atoms can be expected to cause appreciable electron scattering. Therefore not only peak C in the experimental spectra also peak B may tentatively be attributed to emission from band extrema. However, the calculated nonrelativistic spectra allowed an identification of the origin of most of the structures observed, and are found to reflect the experimental spectra quite satisfactorily. To perform relativistic calculations of photoemission spectra for this compound is presently not feasible.

The relativistic band structure has been used for a band mapping of HfN, using the direct-transition model. At normal electron emission ($\mathbf{k}_\parallel = 0$) the transitions in the Brillouin zone are restricted to one line in $\mathbf{k}$ space, the Γ–X direction, and we have assumed that only final states of Δ_6 symmetry contribute to the photoemission current. The final-state bands utilized in the band mapping are marked with a thicker line in Fig. 1. Their nonrelativistic counterpart is a band with Δ_1 symmetry, which lies somewhat higher in energy, as seen in Fig. 1. The experimental energy dispersions determined using spectra recorded at photon energies in the range 17–30 eV are in Fig. 6 compared with the calculated bulk-band structure. Solid circles indicate the location of peaks that can be explained by direct bulk-band transitions. Open circles denote structures that cannot be attributed to direct transitions. Theoretically, transitions are allowed from all initial Δ_6 and Δ_7 bands, but, as seen in Fig. 6, only transitions from the relativistic counterparts to the nonrelativistic Δ_1 and Δ_5 bands are actually observed. The band derived from peak A originates from the Δ_6 and Δ_7 bands, which are fairly narrow (approximately 1 eV). The band derived from peak D originates from the lower Δ_6 band. However, transitions from the uppermost Δ_6 and Δ_7 bands dispersing towards the Fermi level are expected from the calculations, but experimentally only a weak peak showing no dispersion and no polarization dependence could be observed. No structure originating from the Δ_7 band, corresponding to the nonrelativistic $\Delta_{2'}$ band, is observed in the recorded spectra. A trend, already recognized, in this group of transition-metal nitrides is that the deeper-lying bands are generally found at larger binding energies experimentally than what calculations predict for the (100) surfaces.[23–25] The experimental bands closest to the Fermi level are, on the other hand, generally found somewhat closer to the Fermi level, if they are observed at all. These trends are followed also for HfN(100), for which the experimental bands are found deeper below the Fermi level than are the calculated bands. The experimental Δ_6 and Δ_7 bands (peak A) are about 1 eV below the calculated bands at the Γ point and the Δ_6 band (peak D) is about 0.6 eV below the calculated result at the band minimum. The experimental and calculated dispersions of the bands agree reasonably well for those parts of the bands that could be mapped out. The steep part of the Δ_6 band when approaching Γ was not possible to follow. At the photon energies used, the initial and final bands involved then have large slopes and become almost parallel, allowing transitions to occur over wide energy range, resulting in a large width and low intensity of the peak.[26] Peaks B and C give rise to very flat bands that have no counterpart in the calculated band structure. Thus, the appearance of these peaks does

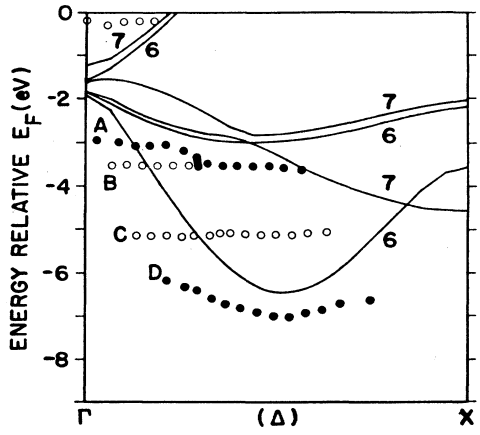

FIG. 6. Comparison between the experimentally determined peak positions and the bulk bands calculated relativistically. Solid circles represent positions of peaks interpreted as originating from direct transitions, while open circles represent transitions that cannot be explained by direct transitions. See text for details.

not involve direct transitions. Off-normal-emission spectra recorded at photon energies of 21.2 and 16.8 eV,[21] moreover, indicate that these peaks cannot be interpreted as three-dimensional density-of-states features. In Figs. 3–5, peaks *B* and *C* are seen to show no dispersion but a polarization dependence, and to become more prominent at higher photon energies. These observations lead us to conclude that these structures arise from emission from band extrema.

Occupied defect states seem to be a common property among the TMCN's. However, no vacancy-induced peaks are observed in the spectra for this $HfN_{0.93}(100)$ single crystal or in the previous x-ray measurements.[4–6] This is somewhat surprising, since the lattice contains 7% nitrogen vacancies, and vacancy-induced peaks have previously been identified for the (100) surface of TiN, ZrN, and VN.[23,25,27] Peaks due to occupied vacancy states have also been observed for the (100) surface of VC and NbC.[28,29] There could be several reasons why such peaks are not observed in HfN. The vacancy concentration could be insufficient or the cross section for vacancy-induced states could be too low. We do not believe, however, that the surface stoichiometry is different from that of the bulk.[30] The lack of resonance effects at the energies used could also be a reason why such defect states are not observed. The resonances observed in VN and ZrN were found to increase the intensity of the vacancy-induced peak.[25,27]

SUMMARY

The band structure of stoichiometric HfN calculated both relativistically and nonrelativistically in the $\Gamma-X$ direction using the LAPW method was presented. The calculated results were used to interpret experimental angle-resolved photoemission spectra from $HfN_{0.93}(100)$, recorded using photon energies in the range 17–56 eV. Theoretical photoemission spectra, calculated nonrelativistically, for stoichiometric composition were presented and a comparison showed that the calculated spectra were able to reproduce most of the experimental structures fairly well. Thus, the nonrelativistic symmetry selection rules describe the observed polarization effects well, despite presence of the heavy hafnium cores. The experimental bulk-band dispersions along the $\Gamma-X$ direction were mapped out, using the direct-transition model and the calculated relativistic band structure. The results show that the dispersion of the calculated bands agrees reasonably well with that of the experimental bands. The calculated bands were, however, found to be located about 0.5–1 eV closer to the Fermi level than the experimentally determined bands.

ACKNOWLEDGMENTS

We gratefully acknowledge the assistance of the staff at the Daresbury Laboratory storage ring. This work was financially supported by the Swedish Natural Science Research Council.

[1]K. Schwarz, Crit. Rev. Solid State Mat. Sci. **13**, 211 (1987).
[2]L. I. Johansson and C. G. Larsson, in *Angle Resolved Photoemission,* edited by S. D. Kevan (Springer, Berlin, 1989).
[3]L. E. Toth, *Transition Metal Carbides and Nitrides* (Academic, New York, 1971).
[4]P. Steiner, H. Höchst, J. Schneider, S. Hüfner, and C. Politis, Z. Phys. B **33**, 241 (1979).
[5]A. J. Perry and L. Schlapbach, Solid State Commun. **56**, 837 (1985).
[6]A. J. Perry, L. Schlapbach, and W. D. Sproul, Solid State Commun. **62**, 23 (1987).
[7]A. N. Christensen, W. Kress, M. Miura, and N. Lehner, Phys. Rev. B **28**, 977 (1983).
[8]The computer program for the band-structure calculation was written by P. E. S. Persson; see P. E. S. Persson, Ph.D. thesis (No. 147), Linköping University, Linköping, 1986.
[9]P. Hohenberg and W. Kohn, Phys. Rev. **136**, B864 (1964).
[10]L. Hedin and B. I. Lundqvist, J. Phys. C **4**, 2064 (1971).
[11]O. K. Andersen, Phys. Rev. B **12**, 3060 (1975).
[12]J. F. L. Hopkinson, J. B. Pendry, and D. J. Titterington, Comput. Phys. Commun. **19**, 69 (1980).
[13]C. G. Larsson, Ph.D. thesis, Chalmers University of Technology, Gothenberg, 1982.
[14]L. I. Johansson, C. G. Larsson, and A. Callenås, J. Phys. F **14**, 1761 (1984).
[15]C. G. Larsson, L. I. Johansson, and A. Callenås, Solid State Commun. **49**, 727 (1984).
[16]P. Weinberger, C. P. Mallett, R. Podloucky, and A. Neckel, J. Phys. C **13**, 173 (1980).
[17]J. Hermanson, Solid State Commun. **22**, 9 (1977).
[18]W. Eberhardt and F. J. Himpsel, Phys. Rev. B **21**, 5572 (1980).
[19]G. Borstel, W. Braun, M. Neumann, and G. Seitz, Phys. Status Solidi B **95**, 453 (1979).
[20]G. Borstel, M. Neumann, and M. Wöhlecke, Phys. Rev. B **23**, 3121 (1981).
[21]J. Lindström, L. I. Johansson, P. E. S. Persson, and A. Cellenås, Z. Phys. B (to be published).
[22]T. Grandke, L. Ley, and M. Cardona, Phys. Rev. B **18**, 3847 (1978).
[23]J. Lindström, P. A. P. Lindberg, L. I. Johansson, D. S. L. Law, and A. N. Christensen, Phys. Rev. B **36**, 9514 (1987).
[24]L. I. Johansson, A. Callenås, P. M. Stefan, A. N. Christensen, and K. Schwarz, Phys. Rev. B **24**, 1883 (1981).
[25]J. Lindström, L. I. Johansson, A. Callenås, D. S. L. Law, and A. N. Christensen, Phys. Rev. B **35**, 7891 (1987).
[26]T.-C. Chiang, J. A. Knapp, M. Aono, and D. E. Eastman, Phys. Rev. B **21**, 3513 (1980).
[27]P. A. P. Lindberg, L. I. Johansson, J. Lindström, and D. S. L. Law, Phys. Rev. B **36**, 939 (1987).
[28]P. A. P. Lindberg and L. I. Johansson, Z. Phys. B **68**, 83 (1987).
[29]P. A. P. Lindberg, L. I. Johansson, J. Lindström, P. E. S. Persson, D. S. L. Law, and A. N. Christensen, Phys. Rev. B **36**, 6343 (1987).
[30]C. Oshima, M. Aono, T. Tanaka, and S. Kawai, Surf. Sci. **102**, 312 (1981).